Loki – A Lava Lake in Rarefied Circumplanetary Cross Flow

Andrew C. Walker, David B. Goldstein, Philip L. Varghese, Laurence M. Trafton, and Chris H. Moore

University of Texas at Austin, Center for Aeromechanics Research, 1 University Station C0600, Austin TX, 78712

Abstract. The interaction between Io's largest hot spot, Loki, and Io's circumplanetary winds is simulated using the direct simulation Monte Carlo (DSMC) method. Our three-dimensional simulation models the rarefied pressure-driven boundary layer flow over a "hot" disk in the presence of a weak gravitational field. The pressure gradient which forces winds away from the subsolar point toward the nightside is caused by the variation in insolation over the surface. The rarefaction varies strongly with time of day due to the exponential dependence of the vapor pressure on the surrounding surface frost temperature ($Kn_{HS} \approx 1\times10^{-4}$ to 0.5 where $Kn_{HS} = \lambda/R$, λ is the mean free path, and R is Loki's effective radius). The spread of heat from the hot spot, the equilibration of pressure over the hot spot, and separation of the boundary layer are examined. The spread of heat away from the hot spot is approximately controlled by $\delta = t_{RAD}U/R$ (t_{RAD} is the radiation time scale and U is the mean wind speed). For cross flow speed considered here, $\delta \approx 0.5$ and therefore the gas warmed by the hot spot cools by $e^{-1} \sim 0.5R$ downstream of the hot spot edge. For the cases without plasma heating, the boundary layer flow separates near the hot spot because the spot creates a significant adverse pressure gradient. Despite the near surface pressure over the hot spot being lower than over surrounding regions, the increased scale height due to the 332 K surface temperature results in higher pressures above the hot spot than the surrounding sublimation atmosphere at high altitudes (>10 km). When plasma heating from above is included the atmosphere is significantly inflated leading to a higher pressure gradient at all altitudes and therefore higher flow speeds. The elevated pressure at high altitudes also decreases the relative size of the adverse pressure gradient created by the hot spot; therefore the boundary layer remains attached. The pressure over the hot spot does not equilibrate with the surrounding sublimation atmosphere because $d_{B\text{-}ATM} < R$ and $d_{B\text{-}HS} > R$ (where $d_{B\text{-}HS}$ is the ballistic length scale over the hot spot); i.e. SO_2 molecules from the local sublimation atmosphere penetrate only $d_{B\text{-}ATM}/R$ into the hot spot and the majority of those molecules will hop back outside the hot spot in a single ballistic trajectory.

Keywords: Io, Atmospheric dynamics.
PACS: 96.12.Jt, 96.30.L-, 96.30.Ib

INTRODUCTION

Io, the innermost Jovian satellite, is the most volcanically active body in the solar system due to tidal flexing resulting from its orbital resonance with Europa and Ganymede. Lava lakes, lava flows, and warm calderas (often called hot spots) are common features on the surface due to this tidal flexing. Many of these features are also sources for volcanic plumes. One of the most prominent hot spots is the lava lake Loki. Observations have determined that the Loki volcanic region accounts for between 30% [1] and 36% [2] of the total heat flow from Io. Marchis *et al*. [2] used the Keck telescope to observe Loki and calculate an effective temperature of 325-340 K and an effective area of $10.3\text{-}11.5\times10^3$ km^2.

Io has also been observed to have a rarefied atmosphere in which the dominant dayside species is SO_2. The two primary sources of the atmosphere are volcanic plumes and sublimating SO_2 surface frosts; however, the dominant source has not yet been determined due to conflicting observations. Pressure gradients in the sublimation atmosphere (due to the variation in insolation) drive circumplanetary flow which diverges in all directions away from the peak pressure region near the subsolar point (the point nearest the sun) toward the nightside.

Io's rarefied atmosphere has been modeled many times before; the first model was proposed in 1985. Ingersoll *et al*. [3] vertically integrated and solved the conservation equations to find sublimation-driven flow. In 1989, Ingersoll

modified the earlier work to account for the non-uniform surface properties [4]. The key idea was the introduction of a horizontal averaging length scale over which any surface frost patches would locally control the surrounding atmospheric pressure. Later models have included radiative transfer, plasma heating, photo- and neutral chemistry [5-9]. All of these simulations modeled Io's atmosphere as a continuum; this is a poor approximation in rarefied conditions (near the nightside and at high altitudes) and a rarefied gas dynamics method such as DSMC must be applied. More recently, Io's atmosphere has been modeled using the DSMC method [10-13].

In the present paper, we examine the rarefied pressure-driven boundary layer flow of the atmosphere over a "large" but finite hot region (Loki) and expand on the previous work of Walker *et al.* [12] which modeled only the sublimation-driven flow without hot spots.

MODEL

To properly account for physics that occurs on Io's surface and in its atmosphere, we have made significant changes and additions to the original DSMC code developed by Bird [14]. These improvements have been documented in detail in earlier work by Walker *et al*. [12]. A brief summary of the additions follows.

SO_2 molecules undergo a gravitational body force consistent with Io's gravity causing them to follow ballistic trajectories after they are sublimated from surface frosts. The SO_2 rotational energy states are treated as continuous while the vibrational energy states are treated as discrete. These energy states are initially populated by assuming that sublimated molecules are in thermal equilibrium with the surface frost. Energy exchange between translation, rotation, and vibration can occur during collisions. Radiation from the internal energy states also occurs via spontaneous emission but all photons are lost since the atmosphere is assumed optically thin. Plasma bombardment by ions and electrons (from the Jovian plasma torus) is modeled via an energy flux. The energy flux is initialized to 1.3 erg/(cm^{2}s) [15] at the top of each column of cells, travels radially downward, and is absorbed by gas in each cell dependent on its SO_2 density. The energy absorbed by the gas goes into rotation and translation while excitation of vibrational modes is neglected. A more physically accurate model for plasma bombardment (which tracks ions and electrons) has been developed and is being tested for use in the three-dimensional DSMC code [16].

Hot Spots & Sublimation Atmosphere

Loki is approximated as a circular disk with an area of 10.8×10^3 km^2 and a uniform surface temperature of 332 K. Loki's actual location on Io has been altered to allow for easier computation; here Loki is located on the equator at 45° W longitude (Loki's actual location is 10° N, 310° W). The hot spot disk is assumed to not sublimate since SO_2 surface frosts would rapidly be burned off by the warm surface temperatures. Some "hot spots" are also known volcanic plumes and have a significant mass flux; we assume that the mass flux from Loki is zero since it is known to be a periodic volcano with quiescent intervals. SO_2 molecules which impact the disk of the hot spot are desorbed during the same time step since the residence time at 332 K is on the order of 10 μs (much smaller than the simulation time step of 0.5 s). Molecules that impact the hot spot surface desorb in thermal equilibrium with the surface. The level of rarefaction over the hot spot can be characterized by defining a "hot spot" Knudsen number ($Kn_{HS} = \lambda/R$) where λ is the mean free path in the local surrounding sublimation atmosphere and R is the effective radius of the "hot spot".

One characteristic length scale of the sublimation atmosphere is the scale height, $H = kT/Mg$. Here k, T, M, and g are Boltzmann's constant, translational gas temperature, molecular mass, and gravitational acceleration, respectively. An atmospheric Knudsen number can then be defined; $Kn_{ATM} = \lambda/H$. For typical surface frost temperatures, the scale height near the surface varies between 8.3 km at 115 K and 6.5 km at 90 K. For convenience and clarity, the rarefaction will generally be defined by Kn_{HS} rather than Kn_{ATM} (with Kn_{HS} a factor of 6 to 8 smaller than Kn_{ATM} at low altitudes).

Simulation Parameters

The DSMC simulations are computed in parallel (with domain decomposition only in azimuth) using a fully three-dimensional spherical grid. The domain covers longitudes between 0° W and 90° W, latitudes between 5° S and 5° N, and up to 400 km in altitude. The lateral (azimuthal and polar) cell size is 1.6 km (1800×200 cells) while the radial cell size grows exponentially with altitude to resolve the mean free path. The radial cell size is ~5 m near the surface but is limited to 5 km at high altitudes. There are 190 radial cells in total. The domain is decomposed in longitude across 360 processors. The boundary condition on the top surface of the domain is a vacuum boundary condition as a negligible number of molecules reach this altitude and are lost. The boundary conditions at 5° S and 5° N are specular reflection. The boundary condition at 0° W located near the peak pressure region is a specular

boundary while the boundary condition at 90° W is a vacuum (since the nightside atmosphere there is essentially collisionless; $Kn_{ATM} > 1$). The lower surface boundary condition is more sophisticated than the other surfaces and is explained in detail in the next section. The constant latitude size domain closely match the global wind speeds computed in Walker *et al.* [12]; however, the actual global winds likely diverge more than the specular boundaries currently allow resulting in some minor non-conformities in the present simulations [12].

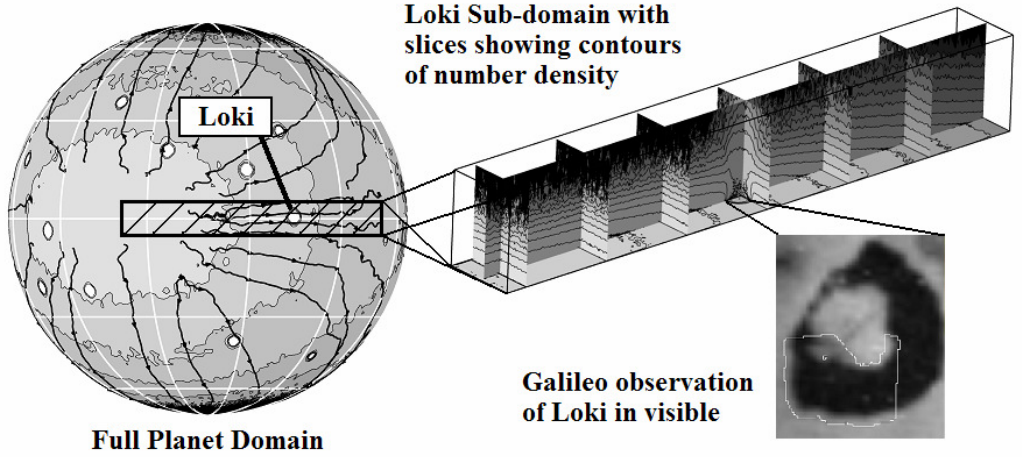

FIGURE 1. The global domain of Io's sublimation atmosphere with a cross-hatched area showing the reduced domain for these circumplanetary flow/hot spot interaction simulations. Loki is visible in the center of the sub-domain (which shows contours of the number density in the atmosphere) and an image of the lava lake taken from Galileo is also shown (the dark area is Loki).

Bottom Surface Boundary Conditions

Io's surface is broken into two separate components: frost and rock. The frost fraction, f_{SO_2}, [17] determines the percentage of frost (and rock) in any given surface cell. The frost and rock surfaces have independent temperatures which differ due to their different albedos and thermal inertias. The number flux of sublimated SO_2 molecules [$(m^2 s)^{-1}$] is a function of the surface frost temperature and the surface frost fraction:

$$N_{SUB} = \frac{1.516\times10^{13} e^{-4510/T_{frost}}}{\sqrt{2\pi k_B T_{frost} M_{SO_2}}} f_{SO_2}. \tag{1}$$

In equation (1) the numerator is the SO_2 vapor pressure [Pa] [18]. The surface frost and rock temperatures are then determined by solving the one-dimensional heat conduction equation with their respective thermal parameters:

$$\rho c \frac{\partial T(\theta,\phi,z,t)}{\partial t} = \frac{\partial}{\partial z}\left[k \frac{\partial T(\theta,\phi,z,t)}{\partial z} \right], \tag{2}$$

where ρ is the density, c is the specific heat, k is the thermal conductivity, t is time, z is the depth into the surface, θ is the latitude, ϕ is the longitude, and T is the surface temperature (rock or frost). The parameters ρ, c, and k can be grouped together to form a single thermal parameter known as the thermal inertia, Γ. The thermal inertia values for the frost and rock are 120 and 30 ergs/cm^{2}Ks$^{1/2}$, respectively based on a best fit to the temperature distribution observed by the Galileo PPR instrument [1]. Five constraints were used to find the best fit to observational data: the mean albedo, the peak brightness temperature, the peak frost temperature, rock thermal inertias lower than frost, and rock albedos lower than the frost. The boundary conditions at the upper surface ($z = 0$) and at a depth where there are no diurnal changes ($z = d$) are given, respectively, by:

$$k \left.\frac{\partial T(\theta,\phi,z,t)}{\partial z}\right|_{z=0} = \varepsilon\sigma T^4(\theta,\phi,z=0,t) - (1-\alpha)\left(F_S(\theta,\phi,t) + F_J(\theta,\phi)\right) - q_{SUB}(\theta,\phi,t) + q_{COND}(\theta,\phi,t), \tag{3a}$$

$$k \left.\frac{\partial T(\theta,\phi,z,t)}{\partial t}\right|_{z=d} = Q_T, \tag{3b}$$

where ε is the emissivity, σ is the Stefan-Boltzmann constant, α is the albedo, F_S is the solar flux, F_J is the reflected flux of sunlight from Jupiter, q_{SUB} and q_{COND} are the heating terms due to the latent heat of sublimation and condensation, respectively, and Q_T is the endogenic heating. The emissivity is assumed to be unity [1]. The frost and

rock albedos are based on the same best fit as the thermal inertias; the albedo values are 0.65 and 0.44, respectively. Modeling of Galileo PPR observations showed that Q_T = 1.0 W/m^2 best fits the data [1].

The frost fraction is also used to determine the probability that a SO_2 molecule will hit frost or rock when it impacts the surface. When molecules impact the frost surface they are deleted because the vapor pressure model assumes a unit sticking coefficient; however, when molecules impact the rock surface they stick for a residence time dependent on the surface rock temperature. The residence time is given by $t_{RES} = \exp(\Delta H_S / k_B T_{rock}) / \nu_0$ [19] where ΔH_S is the surface binding energy of SO_2 on a surface of its own frost ($\Delta H_S/k_B$ = 3460 ± 40 K), and ν_0 is the lattice vibrational frequency ($\nu_0 = 2.4\times10^{12}$ s^{-1}).

RESULTS

Three cross flow cases are investigated. Case 1 is the simplest case and includes homogeneous surface frosts (uniform 50% rock / 50% frost surface) [17], unit sticking on the rock surface, and no plasma heating. Case 2 includes inhomogeneous surface frosts and a residence time on the rock surface but does not include plasma heating. Case 3 includes inhomogeneous surface frosts, a residence time on the rock surface, and plasma heating.

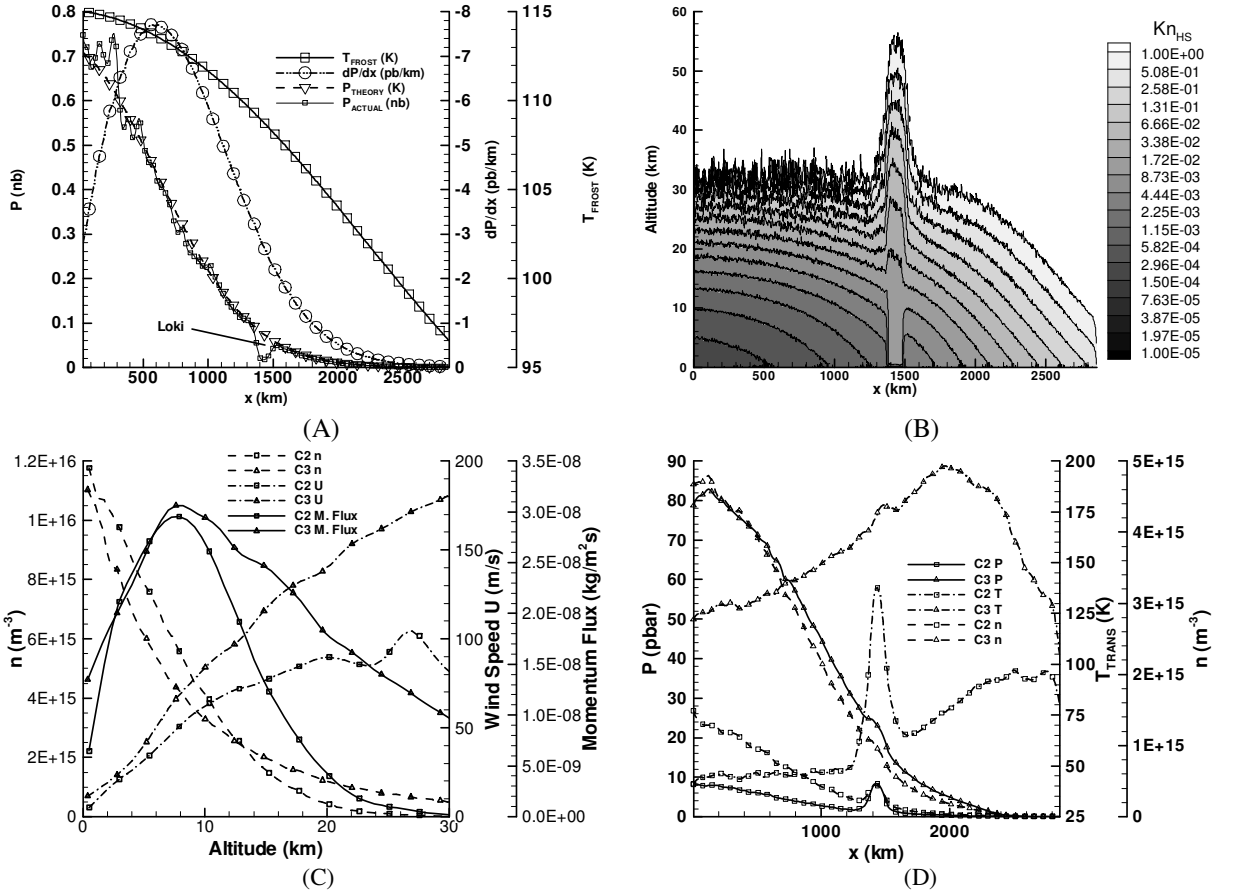

FIGURE 2. (A) The surface frost temperature, pressure above the surface based only on vapor pressure equilibrium (P_{THEORY}), the actual pressure above the surface (P_{ACTUAL}), and pressure gradient (based on P_{THEORY}) as a function of x (the distance away from the peak pressure region) along the equator. The actual gas pressure above the surface tracks vapor pressure equilibrium everywhere but in the vicinity of Loki. (B) Kn_{HS} as a function of altitude and x along the equator. Both A and B are for Case 1. (C) The number density, x-direction wind speed, and x-direction momentum flux for Cases 2 and 3 as a function of altitude. These profiles are taken ~70 km upstream of the upstream edge of the hot spot such that they are outside of the vortex created in Case 2. The x-direction momentum flux is very similar for Case 2 and 3 below 10 km but Case 3 has a much higher x-direction momentum flux above 10 km (~6× greater at 20 km). (D) The pressure, number density, and translational temperature at 20 km as a function of x for Cases 2 and 3. The pressure gradient is much larger in Case 3 than Case 2 resulting in much higher wind speeds and the boundary layer remaining attached.

For Case 1, the pressure gradient creates rarefied boundary layer flow over the "hot spot". The surface temperature varies from ~115 K to ~90 K and therefore the near surface rarefaction varies from $Kn_{HS} \approx 1\times10^{-4}$ to 0.5 (see Figure 2B). At high altitudes $Kn_{HS} >> 1$. The pressure near the surface varies from ~0.7 nbar at peak pressure to ~1 pbar near the nightside. A favorable pressure gradient, $dP/dx < 0$, exists everywhere but in the region near Loki and the flow accelerates monotonically away from the peak pressure region toward Loki. The hot spot surface is a diffuse reflector causing the net x-momentum of the flow to be lost as molecules impact the surface. Furthermore, the mean free path and ballistic length scale are both smaller than the radius of the hot spot ($\lambda < d_{B\text{-}ATM} < R$, where $d_{B\text{-}ATM}$ is the ballistic length scale in the local sublimation atmosphere). The ballistic length scale is defined by $d_{B-ATM} = 8k_B T / \pi mg$ where m is the molecular mass. Thus molecules undergo many collisions along their paths over the hot spot, and the vast majority of molecules will not pass over Loki in a single ballistic trajectory ($d_{B\text{-}ATM} < 2R$). This combination of parameters leads to a moderately collisional ($Kn_{HS} \approx 1\times10^{-3}$) stagnant gas above Loki. The stagnant gas above Loki creates a substantial upstream adverse pressure. Although, the near surface pressure above Loki is lower than that of the surrounding sublimation atmosphere, the pressure becomes higher than the surrounding atmosphere at ~10 km. As the atmospheric flow encounters the large adverse pressure gradient created locally by Loki, the boundary layer separates and a vortex forms (see Figures 3A and 3B). Because of the high x-direction momentum flux of the winds there is significant downstream deflection of the hot gas above the hot spot on the upstream edge. The deflection of the hot spot gas from the vertical is ~35°.

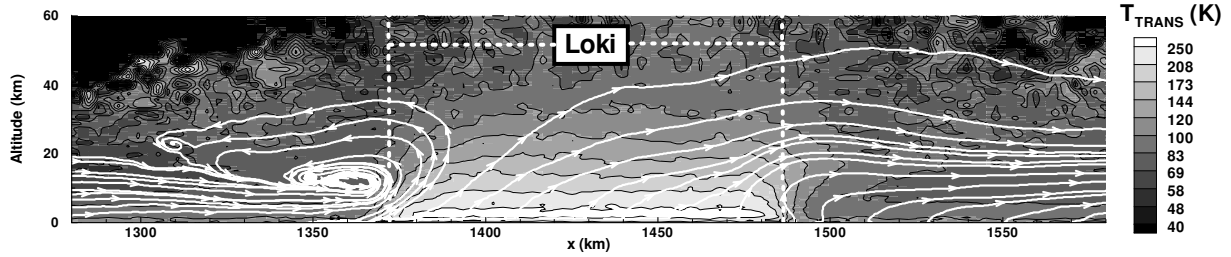

(A) Case 1 – Homogeneous 50:50 frost/rock, unit sticking on rock, no plasma heating

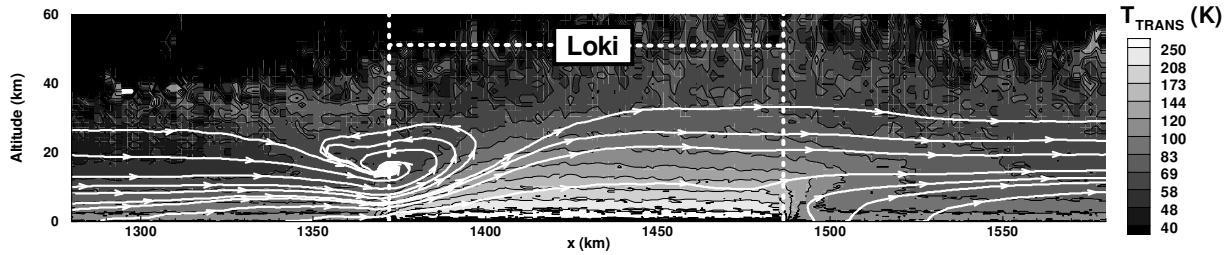

(B) Case 2 – Inhomogeneous frost/rock distribution, residence time on rock, no plasma heating

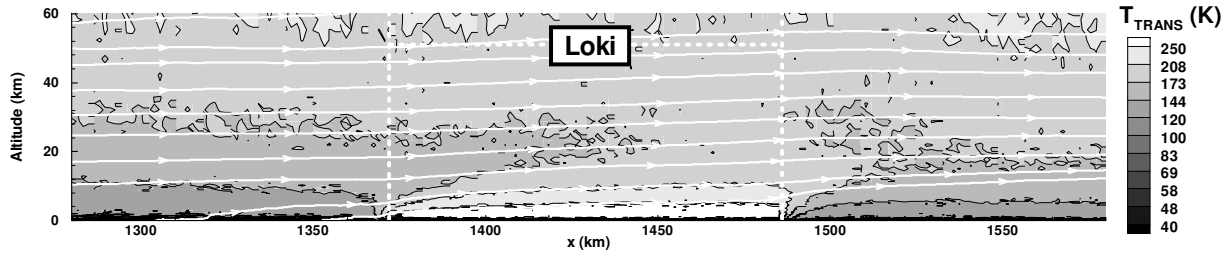

(C) Case 3 – Inhomogeneous frost/rock distribution, residence time on rock, plasma heating (1.3 erg/cm^{2}s)

FIGURE 3. Contours of translational temperature as a function of altitude and distance away from the peak pressure region along the equator. Streamtraces in white show the circumplanetary flow's interaction with the hot spot, Loki. The rarefied boundary layer flow which had developed separates due to the adverse pressure gradient created by the hot spot in Cases 1 and 2. In Cases 1 and 2, streamtraces continue downstream of the hot spot due to three-dimensional effects as the flow curves around the hot spot. In Case 3, the boundary layer flow remains attached.

The situation is largely the same for Case 2. Modeling the residence time on the rock surface slightly increases the day-to-night pressure gradient leading to higher momentum flux in the lower atmosphere. This increases the deflection angle to ~45° (see Figure 3B). For Case 3, the plasma heating significantly alters the dynamics. The

plasma inflates the atmosphere (i.e. higher number densities at higher altitudes); therefore, the atmosphere becomes collisional at higher altitudes. The temperature is also increased by the absorption of plasma energy; however, the effects vary with x because the plasma energy only penetrates a fixed column of gas. The resulting pressures at higher altitudes can be see in Figure 2D. The pressure gradient in Case 3 is much larger than Case 2 and this causes higher flow speeds at higher altitudes (and a higher x-direction momentum flux; see Figure 2C). At high altitudes, the relative size of the adverse pressure gradient created by the hot spot is reduced by the higher pressures due to plasma heating. The pressure gradient remains largely favorable even over Loki and the boundary layer remains attached (see Figures 2D and 3C).

For Cases 1 and 2, the hot gas above Loki forms a wake of warm gas because of the comparable radiation and convection time scales of the SO_2 molecules. A fraction of the molecules that impact the hot spot (and subsequently desorb in thermal equilibrium) will convect downstream with the circumplanetary flow; since $Kn_{HS} \approx 1\times10^{-3}$, collisions will transfer translational energy to the rotational and vibrational energy modes. The energy transferred to vibrational modes is radiated rapidly because the largest Einstein A coefficients of the three SO_2 vibrational modes is 0.88 s^{-1}; therefore, each the vibrational mode radiates most of its energy before the SO_2 molecule travels far from the hot spot ($t_{VIB}U/R \ll 1$, where t_{VIB} is the vibrational radiation time scale). However, the time scale for radiation from the rotational energy states of SO_2, t_{ROT}, is on the order of 250 s at ~300 K ($t_{ROT}U/R \approx 0.5$). The warm gas from Loki cools by e^{-1} after the gas convects ~25 km (or ~0.5R) downstream of the hot spot edge (see Figures 3A and 3B). However, this simplifies the situation a bit as the gas must be collisional to transfer energy away from translation and into the rotational and vibrational internal energy states. At higher altitudes, the collision rate drops slowing the rate at which the translational temperature decreases.

The temperature of the local sublimation atmosphere is significantly increased when plasma heating is included (Case 3). The temperature is high immediately above the surface of Loki but then decreases with altitude due to radiation and adiabatic cooling and then rises again above 20 km where the plasma is able to penetrate (Figure 3C).

For all cases, the pressure over the hot spot does not equilibrate with the local sublimation atmospheric pressure because $d_{B\text{-}ATM} < R$. This is in qualitative agreement with Ingersoll *et al.* [4] who defined $L = \sqrt{2\pi}H$ (when the sticking coefficient is unity) as a horizontal averaging length scale over which local frost patches control the pressure. In separate zero pressure gradient simulations, we found that as H is increased, the pressure became more uniform over the hot spot. Since H and $d_{B\text{-}ATM}$ are directly proportional, this is the same as increasing the ballistic length scale. When $d_{B\text{-}ATM} \approx R$, the pressure equilibrates over the hot spot.

ACKNOWLEDGMENTS

This work is supported by NASA PATM Grant #NNX08AE72G and OPR Grant #NNX08AQ49G. Simulations were performed on supercomputers at the Texas Advanced Computing Center (TACC).

REFERENCES

1. J. Rathbun, J. Spencer, L. Tamppari, T. Martin, L. Barnard, and L. Travis, *Icarus* **169**, 127-139 (2004).
2. F. Marchis and 11 colleagues, *Icarus* **176**, 96-122 (2005).
3. A. Ingersoll, M. Summers, S. Schlipf, *Icarus* **64**, 375-390 (1985).
4. A. Ingersoll, *Icarus* **81**, 298-313 (1989).
5. M. Moreno, G. Schubert, J. Baumgardner, M. Kivelson, D. Paige, *Icarus* **93**, 63-81 (1991).
6. D. Strobel, X. Shu, M. Summers, *Icarus* **111**, 18-30 (1994).
7. M. Wong and R. Johnson, *Icarus* **115**, 109-118 (1995).
8. M. Wong and R. Johnson, *J. Geophysical Res.* **101**, 23243-23254 (1996a).
9. M. Wong and W. Smyth, *Icarus* **146**, 60-74 (2000).
10. J. Austin and D. Goldstein, *Icarus* **148**, 370-383 (2000).
11. C. Moore, D. Goldstein, P. Varghese, L. Trafton, B. Stewart, *Icarus* **201** 585-597 (2009).
12. A. Walker, S. Gratiy, D. Goldstein, C. Moore, P. Varghese, L. Trafton, D. Levin, B. Stewart, *Icarus* **207**, 409-432 (2010).
13. S. Gratiy, A. Walker, D. Levin, D. Goldstein, P. Varghese, L. Trafton, C. Moore, *Icarus* **207**, 394-408 (2010).
14. G. Bird, *Molecular Gas Dynamics and the Direct Simulation of Gas Flows*. Oxford Univ. Press. Oxford, 1994.
15. J. Linker, M. Kivelson, R. Walker, 1988. *Geophys. Res. Lett.* **15**, 1311–1314.
16. C. Moore, H. Deng, D. Goldstein, D. Levin, P. Varghese, L. Trafton, B. Stewart, A. Walker, *Rarefied Gas Dynamics: Proceedings of the 27th International Symposium*, Monterey, CA.
17. S. Douté, B. Schmitt, R. Lopes-Gautier, R. Carlson, L. Soderblom, J. Shirley, Galileo NIMS Team, *Icarus* **149**, 107-132 (2001).
18. D. Wagman, "Sublimation pressure and the enthalpy of SO_2". Chem. Thermodyn. Data Cent., Natl. Bur. of Stand. (1979).
19. S. Sandford and L.J. Allamandola, *Icarus* **106**, 478-488 (1993).